On the temperature structure parameter and sensible heat flux over Helsinki from sonic anemometry and scintillometry

Wood CR[1*], Kouznetsov RD[1,3], Gierens R[1,2], Nordbo A[2], Järvi L[2], Kallistratova MA[3], Kukkonen J[1]

[1] Finnish Meteorological Institute, Erik Palménin aukio 1, FI-00101, Helsinki, Finland

[2] Department of Physics, University of Helsinki, FI-00014, Helsinki, Finland

[3] A.M. Obukhov Institute of Atmospheric Physics, Moscow, Russia

* Corresponding author: curtis.wood@fmi.fi

Keywords

Large-aperture scintillometer, structure parameter, sensible heat flux, urban climate, area-average turbulence, turbulence observations

Abstract

Two commercial large-aperture scintillometers, Scintec BLS900, were tested on path lengths of 1840 m and 4200 m at about 45–65 m above ground, in Helsinki. For July 2011 through June 2012 we observed large variability in diurnal and annual cycles of both temperature structure parameter, C_{T}^2, and sensible heat flux, H. Scintillometer data were compared with data from two eddy-covariance stations. A robust method was developed for the calculation of C_{T}^2 from raw sonic-anemometer data. In contrast to many earlier studies, which solely present the values of H, the main focus here is on comparisons of C_{T}^2 itself. This has advantages, because optical-wavelength scintillometers measure C_{T}^2 with few assumptions, while the determination of H implies the applicability of Monin-Obukhov Similarity Theory that has several inherent limitations. The histograms of C_{T}^2 compare well between sonic and scintillometer. In-depth analysis is focused on one of the scintillometer paths: both C_{T}^2 and H comparisons gave similar and surprisingly high correlation coefficients (0.85 for C_{T}^2 and 0.84–0.95 for H in unstable conditions) given the differences between the two measurement techniques, substantial sensor separation, and different source areas.

1. Introduction

The scintillometry method is based on atmospheric refraction. For optical waves, the refraction is dominated by atmospheric temperature fluctuations, so one can confidently obtain the structure parameter of temperature (C_{T}^{2}). The understanding of C_{T}^{2} itself is important for astronomical seeing and ground-to-satellite communications (Travouillon et al. 2003; Tunick 2005), as well as understanding turbulence itself (Coulter and Doran 2002). But the emphasis in scintillometer studies is to estimate sensible heat flux, H. Scintillometry is desirable because it gives a path-average (most typically over some hundreds of meters) which is comparable to the scales typically used in meteorological modeling. Due to the spatial averaging, it is possible to obtain estimates of turbulence quantities over shorter time periods than is possible with the eddy-covariance (EC) method (Aubinet et al. 2012). Yet, the most common way to examine the reliability of scintillometer data is to compare them with local single-point data from sonic anemometers (Andreas 2012; Beyrich et al. 2012; Evans et al. 2012).

The derivation of H from C_{T}^{2} requires many additional assumptions of the nature of turbulence (Moene 2003). These assumptions include the validity of Monin-Obukhov Similarity Theory (MOST), which is valid for a horizontally-uniform surface layer and of questionable validity above it. The application limits of MOST for scintillometry flux measurements above the surface layer have not been thoroughly addressed to date (Beyrich et al. 2012). Moreover, despite the fact that scintillometry gives quite promising results for large heat fluxes in the convective atmospheric boundary layer (Moene et al. 2009), its performance for small sensible heat fluxes (especially under stable stratification even in the surface layer) is not very good (Andreas 2012). The stable cases are of special interest for air quality applications, since small changes in stratification can result in substantial changes in turbulent mixing. Since C_{T}^{2} is a function of turbulent dissipation rates (Monin and Yaglom 2007, chapter 8, item 21), it provides information on turbulence and thus the direct use of C_{T}^{2} is desirable in applications such as numerical modeling. To approach this problem, the understanding of the behavior of C_{T}^{2} over various terrains is needed.

Whilst scintillometry has been widely applied over grassland and cropland, and some of those studies have been over heterogeneous terrain (e.g. Schüttemeyer et al. 2006; Ezzahar et al. 2007; Ward et al. 2011), only few scintillometry studies have been performed over cities (Kanda et al. 2002; Lagouarde et al. 2006; Roth et al. 2006; Masson et al. 2008; Pauscher 2010; Salmond et al. 2012; Zieliński et al. 2012, Wood et al. 2013b). Cities cause difficulties in the interpretation of scintillometer data given the possible heterogeneous surface below the path, in particular the difficulty in determining effective height (including knowledge of the zero-plane displacement height). Furthermore, all studies over cities have been conducted in mid-latitude cities. Therefore, our aim is to understand C_T^2 and scintillometer results over less-well-studied urban terrain at high latitude, given the interest in stable flow over cities (Kukkonen et al. 2005).

In the future, if a model–measurement inter-comparison is to be done, one desires a purely measured quantity to compare with a purely modeled one. For the case of scintillometer-derived fluxes, one compares a flux derived with MOST using experimental values of a stability parameter with a flux derived with MOST using a modeled stability parameter. It would rather be desirable to compare measured C_T^2 (e.g. from sonic anemometers, scintillometers, or acoustic remote sensing) with C_T^2 somehow derived from a model. For such a comparison, one has to be sure that C_T^2 is a reproducible parameter, at least in measurements, i.e. that measured C_T^2 is representative for some area around the measurements. Thus the research question is "How reproducible is C_T^2 at various scales in the urban environment?".

In this paper, we report: (i) the first results from many months' data from two scintillometers and compare them with data from two sonic anemometers over Helsinki, Finland; and (ii) the evaluation of an algorithm for obtaining C_T^2 from sonic anemometers.

2. Materials and methods

a. Instrumentation and site description

Two large-aperture scintillometers (BLS900, Scintec AG, Germany) and two sonic anemometers (USA-1, Metek GmbH, Germany) have been part of a suite of equipment installed across the city of Helsinki, Finland, on the coast of the Gulf of Finland (Fig. 1, Table 1). They are a part of the Helsinki Urban Boundary-layer Atmosphere Network (UrBAN, http://urban.fmi.fi, Wood et al. 2013a) with increasing activity in observing the urban boundary layer in particular since 2004. The site is characterized by the vicinity of the sea and the strong seasonality in climate, caused by the high latitude (>60°N) and semi-continental climate. Downtown Helsinki is located in a peninsula protruding southwards (Fig. 1a), including the sites of Torni, Sitra, and Elisa. Most of the land area on the map is 5–15 m above mean sea level (a.s.l.), with some hills up to about 30 m.

It is desirable to have near-horizontal scintillometer paths given that C_T^2 depends on height: e.g. $C_T^2 \propto z^{-4/3}$ for the free-convection limit (see later). The first scintillometer with a path-length of 4.2 km (hereafter "city-scale scintillometer") has been in operation since 5th July 2011. Its transmitter is located on Hotel Torni in downtown Helsinki, and a sonic is operating just above the transmitter (Nordbo et al. 2012a). The receiver of the city-scale scintillometer is in Kumpula on the Finnish Meteorological Institute (FMI) roof. Nearby is the semi-urban SMEARIII-Kumpula mast with a sonic at the top (Järvi et al. 2009). The mean height a.s.l. of the ground under the scintillometer path is 12.0 m (±8.2 m st. dev.), and mean building height a.g.l. is 16.0 m (Fig. 1b). The second scintillometer, with a 1.8 km path (hereafter "downtown scintillometer"), has been in operation since 1st March 2012. Its transmitter is on the Elisa lattice mast; its receiver is on the Sitra building. This path is over the densely-packed downtown (Fig. 1d), where mean building height a.g.l. is 18.2 m and the ground height a.s.l. is 9.0 m (±3.8 m). The beam and land slopes are such that westerly winds will result in higher effective heights than easterly winds by about 10 m.

The 10 Hz sonic anemometer time series, of the three components of wind and of sonic temperature (i.e. virtual temperature), were used to calculate turbulent fluxes: friction velocity (u_*) and H, in addition to the Obukhov length (L). All flux data were corrected for a range of standard effects, including moisture (Nordbo et al. 2012b). Sonic data were subset into two groups: one with basic quality assurance (only de-spiked), and one with stringent quality assurance according to flux non-stationarity (Foken and Wichura 1996) and possible flow distortion from the mounting mast/building (at Torni for wind directions of 50–185° and for 0–50° at SMEARIII-Kumpula).

b. Obtaining structure parameter from scintillometers

The mean square difference of a conservative scalar X between two points r_1 and r_2 is proportional to the 2/3 power of the distance between the points (Monin and Yaglom 2007, chapter 8, item 21.6), within locally homogeneous isotropic turbulence:

$$(X_1 - X_2)^2 = C_X^2 (r_1 - r_2)^{2/3} . \tag{1}$$

The proportionality coefficient C_X^2 is called a structure parameter of the scalar X.

The small fluctuations of the signal intensity in large-aperture scintillometers provide a means to measure the structure parameter of the optical refractive index (Tatarskii 1971; Clifford et al. 1974):

$$C_n^2 = 1.21 \sigma_{\ln I}^2 D_t^{7/3} R^{-3} , \tag{2}$$

where $\sigma_{\ln I}^2$ is the variance of the logarithm of received intensity, D is aperture size, and R is scintillometer path length.

From 500 Hz light intensity measurements, one-minute averages of the structure parameter of the refractive index of air C_n^2 are calculated by the BLS900 SRun software (version 1.09). To ensure high data quality, any problematic 1-minute data were discarded in our subsequent analyses: error codes are mainly due to (i) insufficient signal caused by rain or fog (0.3% and 0.5% in data from city-scale and downtown scintillometers, respectively) and (ii) power failures and instrument maintenance (24% and 7.3%).

The estimation of C_T^2 from C_n^2 relies on the refractive index being mainly dependent upon temperature, but also humidity and pressure. For dry air, the relationship between C_n^2 and C_T^2 is (Tatarskii 1971)

$$C_\mathrm{T}^2 = \alpha_1^{-2}\left(T^4 / p^2\right)C_\mathrm{n}^2, \tag{3}$$

where T is air temperature, p is atmospheric pressure, and α_1 is a wavelength-dependent proportionality factor. For the BLS900, α_1 = 7.8355·10^{-5} K hPa^{-1} (Scintec 2011). Atmospheric pressure measurements from SMEARIII-Kumpula (HMP243, Vaisala Oyj, Vantaa, Finland) were used for both scintillometers. Air temperature measurements were from Elisa mast (HMP45D, Vaisala Oyj) for the downtown scintillometer, and an average temperature of Elisa and SMEARIII-Kumpula (home-made platinum resistance thermometer Pt-100) masts for the city-scale scintillometer.

The relative error due to humidity in C_T^2 calculated with equation (3) would not exceed 10% for 95% of the current dataset. Nevertheless, in this study the effect of humidity was accounted for by using Wesely (1976):

$$C_\mathrm{T}^2 = \alpha_1^{-2}\left(T^4 / p^2\right)C_\mathrm{n}^2\left(1 - 0.03/\mathrm{Bo}\right)^{-2}, \tag{4}$$

where Bo is the Bowen ratio. The Bowen ratio is calculated as the ratio of sensible to latent heat flux, the latter was derived from flux measurements at SMEARIII-Kumpula and downtown (Torni) sites.

c. Obtaining structure parameter from sonic anemometers

We estimate the structure parameter of temperature from time series of virtual temperature (i.e. uncorrected 10 Hz temperature data directly from the sonic anemometer) by fitting the parameters of model high-frequency spectra proposed by Kouznetsov and Kallistratova (2010). Since that reference is not permanent, we provide further details here.

Within an inertial subrange, the power spectral density of turbulent fluctuations for a scalar follows the '–5/3 law' (Monin and Yaglom 2007). Thus, by applying Taylor's hypothesis to fluctuations of virtual temperature one can write a power spectral density in the temporal domain as:

$$P_{\mathrm{Tv}}(f) = (U/16\pi)C_{\mathrm{Tv}}^{2} f^{-5/3}, \tag{5}$$

where U is a mean wind speed (m s^{-1}) and f is frequency (Hz). High frequencies in observed spectra are usually affected by noise and flattening at high frequencies due to aliasing of frequencies, i.e. the Nyquist effect. To estimate spectra from time series, the Welch periodogram method (Marple 1987) is used. A periodogram is a spectral estimate calculated by averaging the intensities of windowed Fourier spectra for many short segments of the original signal. This averaging, besides the mean values of the spectral density at each frequency, allows one to estimate their statistical uncertainties. Having the spectrum with error-bars, one can fit a model spectrum to it and estimate the accuracy of resulting parameters (Press et al. 2007). For the estimate of a structure parameter, the following model spectrum is used:

$$P_{\mathrm{Tv}}(f) = \alpha\left(f^{-5/3} + (f_{\mathrm{s}} - f)^{-5/3}\right) + \beta, \tag{6}$$

where f_{s} is data sampling frequency (Hz), α and β are fitting coefficients. β gives a spectral intensity of white noise due to random uncertainties in the instantaneous values, and the term $(f_s - f)^{-5/3}$ accounts for the energy folded back from above the Nyquist frequency due to the aliasing effect (FIG. 2). The structure parameter can be estimated from α,

$$C_{\mathrm{Tv}}^{2} = \alpha(U/16\pi)^{-2/3}. \tag{7}$$

The uncertainty of the resulting value can be estimated from the fitting error of α, and the goodness-of-the-fit of the model spectrum can be estimated with the Pearson chi-square test (Press et al. 2007). These values also allow for the quality control of the resulting structure parameters.

For practical calculations of the spectra, we used a one-size-fits-all approach: a fixed segment length of about 10 seconds (128 data points at 10 Hz), which was generally well within the inertial sub-range of turbulence for the heights of several tens of meters. The calculations with the data used for this study have shown small dependence (< 20–30%) of the resulting structure parameters on the segment length within a range from 32 to 1024 points. Too-small segments lead to the decrease of the structure-parameter accuracy at low values, when the spectrum is strongly affected by measurement uncertainties. This effect was most pronounced for low values of the temperature structure parameters. If segments are too long, the signal from beyond the inertial subrange appears in the estimated spectrum. This results in a degradation of fitting performance of the model spectrum (Eq. 6) and corresponding increase in chi-square. The choice of a segment length could be performed with some approximation of turbulent spectra (Kaimal et al. 1972), however, a simpler way is to choose a fixed segment length and then discard the resulting structure parameters that do not meet the quality criteria for the accuracy and goodness-of-fit.

Unlike the earlier methods (Greenhut and Mastrantonio 1989; Beyrich et al. 2005), the model spectrum (Eq. 6) does not require any procedure to select the high-frequency limit of the inertial subrange in measured spectra, but can use the spectra up to the Nyquist frequency. Attenuation of spectra, due to insufficient sensor response at high frequencies, was not observed; however it can be incorporated into the model spectrum. Should this attenuation become substantial, it would be detected with the chi-square test.

In this study the sonic-derived structure parameter data were rejected based primarily on the chi-square test. The main reason for the test failure is too low wind speed that invalidates the Taylor hypothesis for temperature fluctuations. The rejected fractions are 7.6% and 14.2% of all 30-minute-average values for SMEARIII-Kumpula and downtown (Torni), respectively.

C_{Tv}^2 slightly differs from pure C_{T}^2 due to the effect of humidity. Since C_{T}^2 is proportional to the square of temperature fluctuations, the square of the corresponding factor (Schotanus et al. 1983) was applied to get C_{T}^2 from C_{Tv}^2:

$$C_{\mathrm{T}}^2 = C_{\mathrm{Tv}}^2 \left(1 - 0.06/\mathrm{Bo}\right)^{-2}. \tag{8}$$

d. Estimating sensible heat flux from structure parameter

Several methods have been proposed for deriving sensible heat flux from C_T^2 (Hill 1992). Based on MOST, the dimensionless C_T^2 can be expressed as

$$\frac{z'^{2/3}}{T_*^2}C_\mathrm{T}^2 = \phi_\mathrm{CT}\left(\frac{z'}{L}\right), \tag{9}$$

where $L = -u_*^2 T/\kappa g T_*$, $g = 9.8$ m s^{-2} is acceleration due to gravity, $\kappa = 0.4$ is the von Kármán constant, $\phi_\mathrm{CT}(z'/L)$ is a universal function of atmospheric stability, z' is the effective height (introduced later), and the scaling parameter for temperature is

$$T_* = H/(u_* \rho c_\mathrm{p}), \tag{10}$$

where ρ air density (kg m^{-3}), and c_p the specific heat capacity of air at constant pressure (J K^{-1} kg^{-1}). Different expressions for $\phi_\mathrm{CT}(z'/L)$ have been developed (Thiermann and Grassl 1992; Moene 2003), and the effect of the choice on the final flux value is the order of 10–15% (Meijninger et al. 2005). For the present analysis, we use the form (de Bruin et al. 1993)

$$\phi_\mathrm{CT} = 4.9\left(1 - 9\frac{z'}{L}\right)^{-2/3} \quad \text{for } z'/L < 0. \tag{11}$$

Combining equations (9)–(11), an expression for sensible heat flux can be derived; such estimates are hereafter given the 'MO' label (from MOST). Values of u_* and L are used from nearby sonic data and thus iteration is not needed in the calculation of *H*, e.g. as is used in situations where EC data are not available (e.g. Hartogensis et al. 2003).

Under strongly unstable conditions ($z'/L << -0.1$), equations (9) and (11) can be reduced to the asymptotic form (de Bruin et al. 1993, 1995). Combining this asymptotic form with equation (10), H can be estimated without any supplementary turbulence measurements. This is known as the free-convection (FC) limit

$$H_\mathrm{FC} = 0.58\,\rho c_\mathrm{p} z'(g/T)^{1/2}\left(C_\mathrm{T}^2\right)^{3/4}. \tag{12}$$

Measured C_T^2 is assumed as $\int C_T^2(u)\,\mathrm{d}u$ (where u is along-beam distance) to represent different conditions along the beam. However, in the calculation of H, one single height is needed to be representative of the single value of C_T^2. We denote this single height as the effective height, which must account for the zero-plane displacement height under the beam $z_d(u)$, the weighting function $G(u)$, and stability. In unstable conditions (Hartogensis et al. 2003; Lagouarde et al. 2006):

$$z' = \frac{-1 + \sqrt{1 - 4c_2/L\left[\int_0^1 \left\{\left[z(u) - z_d(u)\right]\left[1 - c_2\,\frac{z(u) - z_d(u)}{L}\right]\right\}^{-2/3} G(u)\,\mathrm{d}u\right]^{-3/2}}}{-2c_2/L}, \tag{13}$$

where $c_2 = 9$ is a coefficient from the universal function of atmospheric stability (eq. 11). For the free-convection limit, z' becomes independent of stability and reduces to the form (Hartogensis et al. 2003):

$$z' = \left\{\int_0^1 \left[z(u) - z_d(u)\right]^{-4/3} G(u)\,\mathrm{d}u\right\}^{-3/4}. \tag{14}$$

A formulation for stable stratification also exists (Kleissl et al. 2008) but it is not needed here since we will only calculate H for unstable stratification. The scintillometer effective height takes into account the spatial averaging and the stability dependence. The effective height as defined in the eddy-covariance community is simply the difference between the sonic anemometer height and the zero-plane displacement height in the flux footprint.

Estimates of sensible heat flux are subject to some uncertainty. For greater certainty a source-area-model technique (Kormann and Meixner 2001) could be performed to estimate zero-plane displacement height from morphological techniques (Grimmond and Oke 1999) for different upwind sectors and stabilities (and thus different z' values). Such an analysis was not conducted here, partly due to the questionable source area estimates above urban cities, but one can qualitatively estimate the impact of upwind terrain on the measurement sites. Consequently, estimates of sensible heat flux were limited to the downtown scintillometer where there is more homogeneity in the terrain below that scintillometer beam compared to the city-scale beam (FIG. 1). Estimates for downtown Helsinki (Nordbo et al. 2012a) gave an average zero-plane displacement height of z_{d} = 14.9 ± 3.0 m (± one standard deviation) within the source area of the Torni EC station. The effective height a.g.l. for the downtown scintillometer is 48.3 m, assuming a constant zero-plane displacement height. This estimate has an uncertainty, due to neighborhood variation in z_{d}, in z' of ±6%. For example, this corresponds to a ±6% uncertainty in H when applying the free-convection limit (Eq. 12) and 3% for neutral conditions (Hartogensis et al. 2003). However, the errors would be larger for the city-scale scintillometer path with its more heterogeneous surface (affecting both beam height a.g.l. and zero-plane displacement height). For comparison, the random uncertainty of H from eddy-covariance measurements in Helsinki has been estimated to be 13% (Nordbo et a. 2012a), and the value is very close to the error estimates for a forest site based on a two tower approach and a successive days approach (Hollinger and Richardson 2005).

3. Results

a. Structure parameter from the scintillometers

The variability of C_{T}^2 over Helsinki shows an annual cycle, and distinct diurnal cycle during Spring through Fall (FIG 3a). Most of the largest C_{T}^2 (~10^{-3} – 10^{-1} $\mathrm{K}^2\,\mathrm{m}^{-2/3}$) occurred during daytime unstable conditions. But also, there were a few high values during November, January, and February nights consistent with the large occurrence of negative sensible heat fluxes over Helsinki. Indeed, the sonic-derived sensible heat fluxes were negative for 45% of the time in those particular studied months, partly driven by the long nights and snow-cover (Wood et al. 2013a). The lowest C_{T}^2 values occurred mostly in winter; this is consistent with small diurnal variations in sensible heat flux due to weak insolation, and synoptic conditions of near-continuous cloud cover resulting in a neutrally stratified atmosphere.

Comparing C_{T}^2 between scintillometers (FIG. 3b) showed an agreement within a factor of 2 for most of the data; some difference is not surprising given the higher beam downtown and different source areas of the two instruments. The downtown scintillometer generally showed lower values of C_T^2 (despite having a higher z'), perhaps due to a higher occurrence of neutral cases downtown, when stable stratification occurs at larger scales. The saturation at high C_T^2 is clearly seen for the longer-path city-scale scintillometer and is an instrumental effect (see Appendix A).

b. Comparison of structure parameter from sonic and scintillometer

The ratios $C_T^2(\text{sonic})/C_T^2(\text{scint})$ downtown indicate that the sonic gives on average slightly higher values of C_T^2 than the scintillometer (FIG. 4a) for most wind sectors, although their median difference lies within about 50%; whereas the individual values show a substantial scatter up to a factor of 5–10. For flow-distortion directions, median C_T^2 from the sonic is nearly three times that from the scintillometer, indicating turbulent-wake effects from the sonic's position atop Torni.

The ratio of C_T^2 obtained from the two devices differs also depending on the atmospheric stability. During unstable conditions, the sonic generally gives greater values than the scintillometer and vice versa during stable conditions (FIG. 4b). Though downtown Helsinki is quite homogeneous, the source areas of the sonic at Torni and the downtown scintillometer still differ, and the variation of stratification obviously affects them differently. Another source of discrepancy could be the layered structure of C_T^2 in the stably-stratified atmosphere which enhances the effect of height difference between the sensors (TABLE 1). It is not clear to us if there are any other reasons for such stratification dependency.

A comparison between sonic and scintillometer downtown (FIG. 5a,b) for many days of data shows a good agreement for C_T^2 (r = 0.85). This corroborates the usability of the spectral method to calculate C_T^2 from sonic data and gives confidence to scintillometer and sonic measurements in very complex urban environments with varying ground and canopy height, notwithstanding the uncertainty in effective heights due to lack of source-area estimates. Moreover, the statistical distribution of the observed values of C_T^2 coincides quite well for the downtown scintillometer and the sonic at Torni (FIG. A1).

Two case days demonstrate the time evolution of C_T^2 and H (FIG. 6): (a) clear-sky summertime with high atmospheric pressure (>1020 hPa) and southerly flow, (b) cloudy wintertime with low pressure (<994 hPa) and westerly flow. For the sunny day, there is broad agreement between C_T^2 from all methods. Sensible heat flux, estimated directly from the EC method and indirectly from C_T^2 for different instruments, shows remarkable agreement – especially given the difference between methods and the difference between point and path-average measurements. Interestingly, one can see higher C_T^2 at SMEARIII-Kumpula than downtown overnight – caused by stable stratification. For the winter day, there is much more variation between the C_T^2 datasets, especially in their temporal evolution: at the semi-urban site (SMEARIII-Kumpula) H is near zero, whilst downtown stratification is unstable.

c. Relationship with sensible heat flux

It is not possible to estimate H from C_T^2 alone, as is derived from sonics or scintillometers (FIG. 7). The relationship is clear: low C_T^2 occurs during neutral stratification, but H cannot be unambiguously known given a greater C_T^2 alone. Nevertheless, the free-convection theoretical relationship between H and C_T^2 in unstable conditions (Eq. 12) is followed in the sonic measurements very well despite the complicated surface (FIG. 7b,d). This also applies for the scintillometers except for the saturation effect at high H, especially for the city-scale scintillometer (FIG. 7a,c).

The quality of C_T^2 as a predictor of H is assessed using EC-derived fluxes for unstable stratification when we expect the method to work the best. Four combinations of fluxes derived from C_T^2, sonic/scintillometer, and free-convection/MOST are examined (FIG. 5c–f). For the latter, the stability parameter from the Torni sonic was used. Generally, the scintillometer C_T^2 results give slightly less scatter against *H* from the sonic than the C_T^2 from the sonic itself, and the MOST method gives better agreement than the free-convection method. The better performance of the scintillometer method is caused by a better statistical certainty of the corresponding C_T^2, given the path average compared with the sonic's point measurement. Whilst similarity relationships hold on average, individual values of C_T^2 and H from sonic might be inconsistent, since sampling errors of these quantities are quite high in single-point measurements and not correlated with each other. In the sonic–scintillometer comparison, at least C_T^2 (from scintillometer) is quite well determined. Since scintillometer results give best agreement, credence is given to the notion of homogenous building layouts downtown, i.e. even though the footprints do not always overlap the scintillometer-derived C_T^2 still gives slightly better agreement on H than sonic-derived C_T^2.

These sensible heat flux comparisons are only slightly worse than other scintillometer studies (Lagouarde et al. 2006; Roth et al. 2006; Zieliński et al. 2012): i.e. giving high correlation coefficients of 0.85–0.95, but also rms errors of 20–100 W m^{-2}. Note, however, that the absolute scatter in FIG. 5c–f is mostly caused by larger values of C_T^2 (and fluxes). The performance of C_T^2 methods for H in near-neutral cases is poor in terms of relative error. Due to spatial averaging, one can expect the scintillometer-derived C_T^2 to have good statistics even for small temporal samples.

4. Summary

Measurements were performed in the city of Helsinki using two large-aperture scintillometers (Scintec BLS900) and two Metek USA-1 sonic anemometers. One scintillometer has been installed in relatively homogeneous terrain downtown with a 1.8 km path; the other one has a longer city-scale path and more heterogeneity underneath. Sonics were installed at the end-points of the city-scale scintillometer's path (ideal points near the center of scintillometer beams were not possible due to practical constraints in finding available measurement locations in cities). C_T^2 values obtained from scintillometer data have clear diurnal and annual cycles. The diurnal cycle is most pronounced in summer. Low values of C_T^2, corresponding to neutral stratification, occur downtown much more often than at the city-scale, which is consistent with the heat fluxes above the urban surface (Nordbo et al. 2012a). A consistency in C_T^2 data between the downtown and city-scale scintillometers was nevertheless observed, despite the difference in their effective heights.

A robust method to derive C_T^2 from fixed-point high-frequency temperature measurements was developed and tested here. The method provides reliable quality parameters for the resulting values. This robust method was for the first time used for quantitative long-term urban comparisons of scintillometer and eddy-covariance measurements, and good agreement was observed. The method was also used to identify the saturation problem that was observed in cases of strong scintillations (see Appendix A).

The challenges in estimating sensible heat flux from C_T^2 (Moene 2003) were highlighted, given the non-unique solution. A commonly used method, which we employed, to estimate sensible heat flux from C_T^2 relies both on assumptions in MOST and on nearby auxiliary data, and so an advantage is lost by contamination of the fuller utility of the path-average by introducing a point measurement (although estimates of u_* have been made from scintillometer data, e.g. Chehbouni 2000). Even when using MOST, considerable uncertainty results, including uncertainty in effective height: which will always be a challenge for urban areas. There is generally good agreement for sonic–scintillometer comparison, although there is horizontal and vertical separation between the sonic anemometer and the center of the scintillometer beam (giving rise to effective-height and source-area inconsistencies). Furthermore, the rms error found is large enough to result in large absolute uncertainty for near-neutral heat fluxes, a problem also seen in EC flux data given detection limits and uncertainties of order 10 W m^{-2}.

The climate conditions in Helsinki represent a challenge for scintillometry given the urban surface and the high-latitude location giving rise to negative sensible heat fluxes even above an urban surface. The values of sensible heat flux are typically small, which poses a problem to MOST-based methods. Moreover, shallow boundary layers of a few tens of meters that often occur over Helsinki can invalidate the surface layer scaling, which is a prerequisite of MOST. In such cases, a surface layer might not exist.

A challenge now presents itself: how do we make best use of C_{T}^{2} itself in applications such as numerical models of weather prediction and air quality?

Acknowledgements

This work has been supported by the EC FP7 ERC Grant 227915 "Atmospheric planetary boundary layers – physics, modelling and role in Earth system", Academy of Finland (Projects 138328, 1118615, and ICOS-Finland 263149), and Russian Foundation for Basic Research (Project 13-05-00846). Kari Riikonen, Erkki Siivola, Petri Keronen, and Sami Haapanala provided technical support. We are grateful to the reviewers for valuable comments, and to Timo Vesala, Sylvain Joffre, Ari Karppinen, Lukas Pauscher, Helen Ward, Oscar Hartogensis, Daniëlle van Dinther, and Sue Grimmond for fruitful discussions.

Disclaimer

The results and conclusions in this study were made at specific locations and with specific equipment configurations. They should not be used to judge the general performance of instruments or particular manufacturers.

APPENDIX A

Saturation of the scintillometers

To quantify the effect of saturation (Kohsiek et al. 2006) for our scintillometers, the histograms of C_T^2 were plotted for each sonic and scintillometer (FIG. A1). One can see a largely comparable C_T^2 between the two sonic anemometers – with a slight bias towards larger values downtown. And the sonic anemometers show a smooth histogram for C_T^2 values. However, the scintillometer data show a distinct lack of very high C_T^2 values, with a notable pattern: an increase and then decline to zero. This occurs (i) at about 2×10^{-2} K^2 m$^{-2/3}$ for the longer path with a very pronounced transition; and (ii) at about 3×10^{-2} K^2 m$^{-2/3}$ for the shorter path with a less-pronounced transition. The Scintec manual (Scintec 2011) states that the maximum measurable values of C_T^2 for BLS900 are 7 and 0.07 K^2 m$^{-2/3}$ for 2 and 5 km path correspondingly. The manual's limit values are well above the values for which we observed saturation in our instruments. Note, that only the data reported valid, by the Scintec SRun 1.09 software, are used for the histograms. Such behavior is likely caused by inability of the implemented correction (Clifford et al. 1974) to correct all the data affected by saturation. It is not clear if this is an implementation problem or a problem of the correction itself. Most values of C_T^2 in our scintillometer measurements are smaller than 10^{-2} K^2 m$^{-2/3}$, and for them the downtown histograms coincide quite well. We thus consider those data reliable.

References

Andreas, E. L., 2012: Two Experiments on Using a Scintillometer to Infer the Surface Fluxes of Momentum and Sensible Heat. *J. Appl. Meteor. Climatol.*, **51**, 1685–1701.

Aubinet, M., T. Vesala, and D. Papale, 2012: *Eddy Covariance - A Practical Guide to Measurement and Data Analysis*. Springer atmospheric sciences, ISBN13:978-9400723504.

Beyrich, F., R. D. Kouznetsov, J.-P. Leps, A. Lüdi, W. M. L. Meijninger, and U. Weisensee, 2005: Structure parameters for temperature and humidity from simultaneous eddy-covariance and scintillometer measurements. *Meteorologische Zeit.*, **14**, 641–649.

—, and Coauthors, 2012: Towards a Validation of Scintillometer Measurements: The LITFASS-2009 Experiment. *Bound.-Layer Meteor.*, **144**, 83–112.

Chehbouni, A., 2000: Estimation of heat and momentum fluxes over complex terrain using a large aperture scintillometer. *Agric. For. Meteor.*, **105**, 215–226.

Clifford, S. F., G. R. Ochs, and R. S. Lawrence, 1974: Saturation of optical scintillation by strong turbulence. *J. Optic. Soc. Amer.*, **64**, 148.

Coulter R.L. and J. C. Doran 2002: Spatial and temporal occurrences of intermittent turbulence during CASES99. *Bound.-Layer Meteor.*, **105**, 329–349.

de Bruin, H. A. R., W. Kohsiek, and B. J. J. M. van den Hurk, 1993: A verification of some methods to determine the fluxes of momentum, sensible heat, and water vapour using standard deviation and structure parameter of scalar meteorological quantities. *Bound.-Layer Meteor.*, **63**, 231–257.

—, B. J. J. M. van den Hurk, and W. Kohsiek, 1995: The scintillation method tested over a dry vineyard area. *Bound.-Layer Meteor.*, **76**, 25–40.

Evans J. G., and Coauthors, 2012: Determination of turbulent heat fluxes using a large aperture scintillometer over undulating mixed agricultural terrain. *Agric. For. Meteor.*, **166–167**, 221–233.

Ezzahar, J., A. Chehbouni, J. C. B. Hoedjes, and A. Chehbouni, 2007: On the application of scintillometry over heterogeneous grids. *J Hydrol.*, **334**, 493–501.

Foken, T., and B. Wichura, 1996: Tools for quality assessment of surface-based flux measurements. *Agric. For. Meteor.*, **78**, 83–105.

Greenhut, G. K., and G. Mastrantonio, 1989: Turbulence Kinetic Energy Budget Profiles Derived from Doppler Sodar Measurements. *J. Appl. Meteor.*, **28**, 99–106.

Grimmond, C. S. B., and T. Oke, 1999: Aerodynamic Properties of Urban Areas Derived from Analysis of Surface Form. *J. Appl. Meteor.*, **38**, 1262–1292.

Hill, R. J., 1992: Review of optical scintillation methods of measuring the refractive-index spectrum, inner scale and surface fluxes. *Waves Rand. Med.*, **2**, 179–201.

Hollinger, D. Y., and A. D. Richardson, 2005: Uncertainty in eddy covariance measurements and its application to physiological models. *Tree phys.*, **25**, 873–885.

HSY, 2008: Seutu CD – a dataset by the Helsinki Region Environmental Services Authority.

Järvi, L. and Coauthors, 2009: The urban measurement station SMEAR III: Continuous monitoring of air pollution and surface-atmosphere interactions in Helsinki, Finland. *Bor. Env. Res.*, **14**, 86–109.

Kaimal, J. C., Y. Izumi, J. C. Wyngaard, and R. Cote, 1972: Spectral Characteristics of Surface-Layer Turbulence. *Quart. J. Roy. Meteor. Soc.*, **98**, 563–589.

Kanda, M., R. Moriwaki, M. Roth, and T. Oke, 2002: Area-averaged sensible heat flux and a new method to determine zero-plane displacement length over an urban surface using scintillometry. *Bound.-Layer Meteor.*, **105**, 177–193.

Kohsiek, W., W. M. L. Meijninger, H. A. R. Debruin, and F. Beyrich, 2006: Saturation of the Large Aperture Scintillometer. *Bound.-Layer Meteor.*, **121**, 111–126.

Kormann, R., and F. X. Meixner, 2001: An analytical footprint model for non-neutral stratification. *Bound.-Layer Meteor.*, **99**, 207–224.

Kouznetsov, R. D., and M. Kallistratova, 2010: Anisotropy of a small-scale turbulence in the atmospheric boundary layer and its effect on acoustic backscattering. *International Symposium for the Advancement of Boundary Layer Remote Sensing. Paris, 28–30 June 2010.* (http://www.isars2010.uvsq.fr/images/stories/Presentations/O_TUR_02_Kouznetsov.pdf)

Kukkonen, J., and Coauthors, 2005: Analysis and evaluation of selected local-scale PM10 air pollution episodes in four European cities: Helsinki, London, Milan and Oslo. *Atmos. Environ.*, **39**, 2759–2773.

Lagouarde, J.-P., M. Irvine, J.-M. Bonnefond, C. S. B. Grimmond, N. Long, T. R. Oke, J. A. Salmond, and B. Offerle, 2006: Monitoring the Sensible Heat Flux over Urban Areas using Large Aperture Scintillometry: Case Study of Marseille City During the Escompte Experiment. *Bound.-Layer Meteor.*, **118**, 449–476.

Marple, S. L., 1987: *Digital Spectral Analysis with Applications*. Englewood Cliffs: Prentice Hall.

Masson, V. and Coauthors, 2008: The Canopy and Aerosol Particles Interactions in TOulouse Urban Layer (CAPITOUL) experiment. *Meteor. Atmos. Phys.*, **102**, 135–157.

Meijninger, W. M. L., F. Beyrich, A. Lüdi, W. Kohsiek, and H. A. R. D. Bruin, 2005: Scintillometer-Based Turbulent Fluxes of Sensible and Latent Heat Over a Heterogeneous Land Surface – A Contribution to Litfass-2003. *Bound.-Layer Meteor.*, **121**, 89–110.

Moene, A. F., 2003: Effects of water vapour on the structure parameter of the refractive index for near-infrared radiation. *Bound.-Layer Meteor.*, **107**, 635–653.

—–, O. K. Hartogensis, and F. Beyrich, 2009: Developments in Scintillometry. *Bull. Amer. Meteor. Soc.*, **90**, 694–698.

—–, W. M. L. Meijninger, O. K. Hartogensis, W. Kohsiek, and H. A. R. de Bruin, 2004: A review of the relationships describing the signal of a Large Aperture Scintillometer. University of Wageningen, Internal Report 2004/2.

Monin, A. S., and A. M. Yaglom, 2007: *Statistical fluid mechanics volume 2: mechanics of turbulence, Dover Publications, Mineola New York, USA*.

National Land of Survey Finland, 2010: Lidar scanning database PaITuli. https://sui.csc.fi/applications/paituli/infra_eng.

Nordbo, A., L. Järvi, S. Haapanala, J. Moilanen, and T. Vesala, 2012a: Intra-city variation in urban morphology and turbulence structure in Helsinki, Finland. *Bound.-Layer Meteor.*, doi:10.1007/s10546-012-9773-y.

—–, —–, and T. Vesala, 2012b: Revised eddy covariance flux calculation methodologies – effect on urban energy balance. *Tellus Ser. B-Chem. Phys. Meteor.*, **64**, 18184.

Pauscher, L., 2010: Scintillometer Measurements above the Urban Area of London. Thesis, University of Bayreuth, Germany. 104 p.

Press, W. H., S. A. Teukolsky, W. T. Vetterling, and B. P. Flannery, 2007: *Numerical Recipes 3rd Edition: The Art of Scientific Computing*. Cambridge University Press, Cambridge, UK.

Roth, M., J. A. Salmond, and A. N. V. Satyanarayana, 2006: Methodological considerations regarding the measurement of turbulent fluxes in the urban roughness sublayer: The role of scintillometery. *Bound.-Layer Meteor.*, **121**, 351–375.

Salmond, J. A., M. Roth, T. R. Oke, A. Christen, and J. A. Voogt, 2012: Can Surface-Cover Tiles Be Summed to Give Neighborhood Fluxes in Cities? *J. Appl. Meteor. Climatol.*, **51**, 133–149.

Schotanus, P., F. T. M. Nieuwstadt, and H. A. R. Bruin, 1983: Temperature measurement with a sonic anemometer and its application to heat and moisture fluxes. *Bound.-Layer Meteor.*, **26**, 81–93.

Schüttemeyer, D., A. F. Moene, A. A. M. Holtslag, H. A. R. Bruin, and N. van Giesen, 2006: Surface Fluxes and Characteristics of Drying Semi-Arid Terrain in West Africa. *Bound.-Layer Meteor.*, **118**, 583–612.

Scintec, 2011: *Scintec Boundary Layer Scintillometer Hardware Manual. Version 2.07. Rottenburg, Germany.*

Tatarskii, V., 1971: *The effects of the turbulent atmosphere on wave propagation (Israel Program for Scientific Translations, Jerusalem) ISBN 07065-0680-4.*

Thiermann, V., and H. Grassl, 1992: The measurement of turbulent surface-layer fluxes by use of bichromatic scintillation. *Bound.-Layer Meteor.*, **58**, 367–389.

Travouillon T., M. C. B. Ashley, M. G. Burton, J. W. V. Storey, R. F. Loewenstein, 2003**:** Atmospheric turbulence at the South Pole and its implications for astronomy. *Astron. Astrophys.,* **400**, 1163–1172.

Tunick, A., 2005: Toward increasing the accuracy and realism of future optical turbulence calculations *Meteor. Atmos. Phys.*, **90**,159–164.

Ward H. C., J. G. Evans, and C. S. B. Grimmond, 2011: Effects of non-uniform crosswind fields on scintillometry measurements. *Bound.-Layer Meteor.*, **141**, 143–163.

Wesely, M. L., 1976: The Combined Effect of Temperature and Humidity Fluctuations on Refractive Index. *J. Appl. Meteor.*, **15**, 43–49.

Wood, C. R. and Coauthors, 2013a: An overview on the Urban Boundary-layer Atmosphere Network in Helsinki. *Bull. Amer. Meteor. Soc.*, **in review**.

Wood, C. R., L. Pauscher, S. Kotthaus, J. F. Barlow, H. Ward, S. Lane, and S. Grimmond, 2013b: Wind observations over the River Thames in central London. *Sci. Tot. Environ.*, **442**, 527–533.

Zieliński, M., K. Fortuniak, W. Pawlak, and M. Siedlecki, 2012: Sensible heat flux in Łódź – scintillometer and eddy covariance measurements. *8th International Conference on Urban Climates*, Dublin, Ireland, ICUC, 4.

TABLE. 1. Instrument positions, see also FIG. 1. Effective heights are as per equation 14 for scintillometers using data in FIG. 1b and d; and directionally averaged $z–z_d$ for sonic anemometers.

Site	**Instrument**	**Co-ordinates**	**Ground height a.s.l. (m)**	**Instrument height a.s.l. (m)**	**Effective height a.g.l. (m)**
Elisa, downtown	Scintillometer transmitter	60.164000° N 24.946667°E	12.0	68.0	48.3
Sitra, downtown	Scintillometer receiver	60.164158°N 24.9140111°E	4.0	72.0	
Torni, downtown	Sonic anemometer	60.167803°N 24.938600°E	15.0	75.2	45
Torni, downtown	Scintillometer transmitter	60.167803°N 24.938600°E	15.0	67.4	33.6
FMI, Kumpula	Scintillometer receiver	60.203644°N 24.960525°E	29.0	52.9	
SMEARIII, Kumpula	Sonic anemometer	60.202817°N 24.961128°E	29.0	60.0	35

List of Figures

FIG. 1. The locations of the instruments in Helsinki. (a) The surface type is in three classes (built/paved (gray), vegetative (green), and water (blue) with 10 m horizontal resolution (HSY 2008)). The city-scale scintillometer is at a bearing of 16° from North, the downtown scintillometer is 271°. FMI is Finnish Meteorological Institute at Kumpula. (b) A birds-eye transect along the city-scale scintillometer beam. Height is that above mean sea level using airborne laser database of 1-meter horizontal resolution (National Land of Survey Finland 2010). (c) A cross-section along the city-scale scintillometer beam. (d) Same as b, but for downtown scintillometer beam. (e) Same as c, but for downtown scintillometer beam.

FIG. 2. An example power spectral density from sonic anemometer data for virtual temperature on 14 May 2011 in downtown Helsinki (at Hotel Torni). Shown with fitted spectra: full model, the model without the aliasing term $(f_s - f)^{-5/3}$, the model with β set to 0, and plain –5/3 spectrum.

FIG. 3. (a) Seasonal and diurnal cycle for 1-minute-mean temperature structure parameter (shaded scale) from the city-scale scintillometer from July 2011 through May 2012. Sunrise and sunset times are marked (black dashed curves). (b) Comparison of 1-minute mean temperature structure parameter values between the two scintillometers March through May 2012, bin averages are superimposed with black squares.

FIG. 4. Ratio of 10-minute-mean data from sonic at Torni to downtown scintillometer during May through June 2012; median values (circles) with 5th and 95th percentiles. (a) For wind-direction bins defined at Torni (flow distortion directions for Torni, 50–185°, are shown as open circles). (b) For stability bins defined at Torni using 30-minute eddy-covariance analysis (flow distortion directions for Torni, 50–185°, are removed).

FIG. 5. 30-minute-mean data for downtown May through June 2012, and bin averages are superimposed with black squares (median y-axis value for x-axis bins); the 1:1 line is shown (dashed). The eddy-covariance (EC) data pass the high-quality tests. (a) Comparison of temperature structure parameter

values between scintillometer and sonic; (b) same as previous subplot, but on linear scale; (c) EC sensible heat flux compared to sensible heat flux using the free-convection (FC) method with scintillometer temperature structure parameter values; (d) same as previous, but with sonic-derived temperature structure parameter; (e) EC sensible heat flux compared to sensible heat flux with the Monin-Obukhov (MO) theory functional form using scintillometer-derived temperature structure parameter; (f) same as previous subplot, but with sonic-derived temperature structure parameter.

FIG. 6. (a) Temporal evolution on 14 May 2012 of temperature structure parameter (1-minute from scintillometers, 10-minute from sonics) and 30-minute H, and (b) 7 January 2012. The legends are the same for horizontal subplots with temperature structure parameter and sensible heat flux. Scint is scintillometer, FC is using the free-convection formulation (Eq. 12), MO is the Monin-Obukhov theory functional form, and EC is using the eddy-covariance method. The EC data pass stringent quality tests (filled circles) or less-stringent quality tests (empty circles). Sunrise and sunset are marked (yellow star).

FIG. 7. Sensible heat flux from 30-minute eddy-covariance (stringent quality tests) on x-axes compared to 30-minute temperature structure parameter for different methods for May through June 2012 on y-axes: (a) downtown scintillometer with downtown (Torni) sonic anemometer; (b) Torni sonic anemometer with same sonic; (c) city-scale scintillometer with sonic anemometers (using a mean of Torni and SMEARIII-Kumpula) (NB. less data due to scintillometer downtime from 24^{th} May onwards); (d) SMEARIII-Kumpula sonic anemometer. Bin averages are superimposed with black squares (median y-axis value for x-axis bins). The free-convection relationship (Eq. 12) is shown with the thick curve.

FIG. A1. Histogram for all the 30-minute periods concurrent in all four instruments. These are thus a subset of days from January, February, May, and June 2012. Scintillometer structure parameters were calculated using local temperature and pressure as per equation 3 (i.e. not Scintec SRun software default). Humidity corrections were not applied.

Figures

(NB. Low quality png files in this .docx. See uploaded eps/pdf files with good fonts & dimensions)

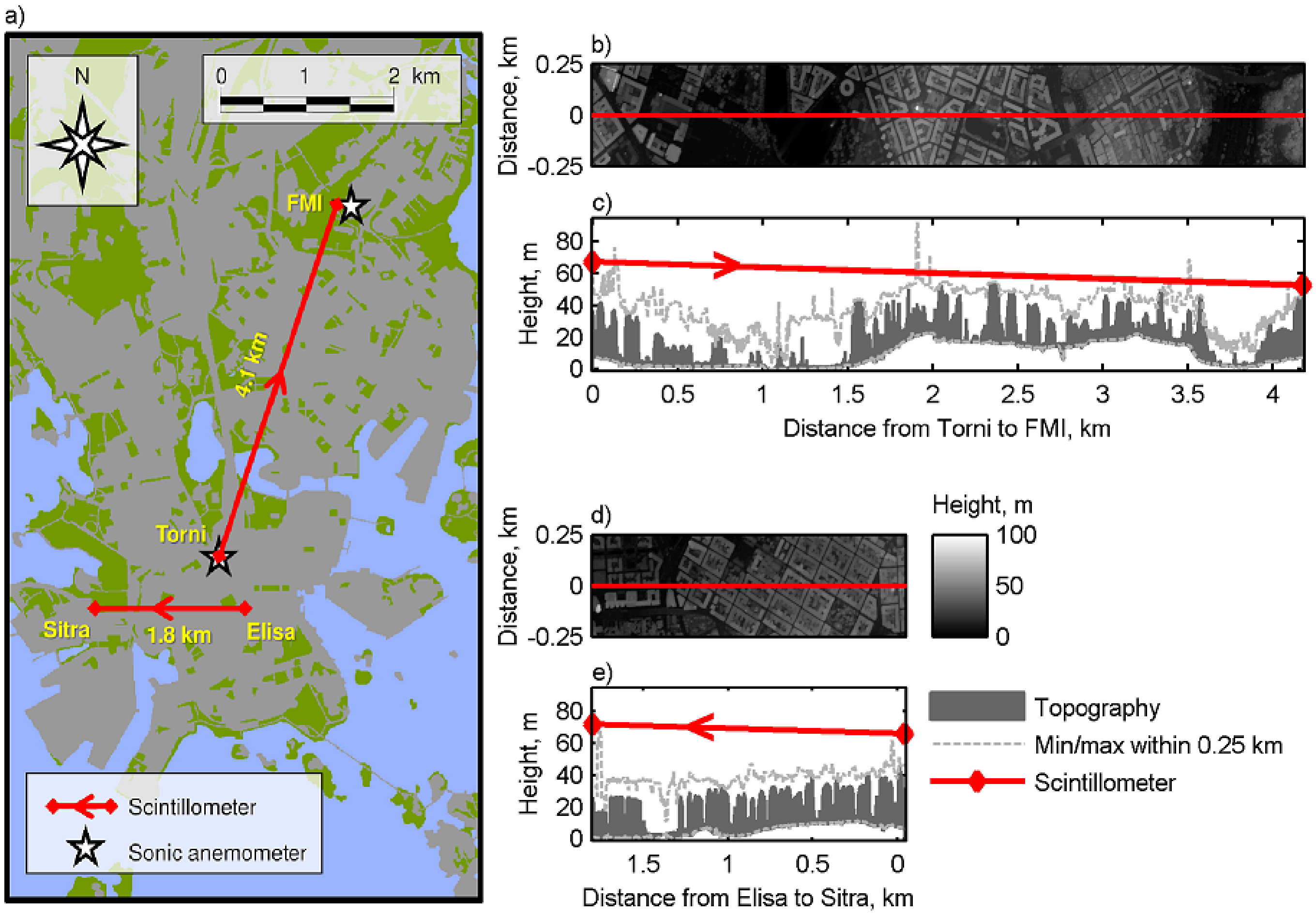

FIG. 1. The locations of the instruments in Helsinki. (a) The surface type is in three classes (built/paved (gray), vegetative (green), and water (blue) with 10 m horizontal resolution (HSY 2008)). The city-scale scintillometer is at a bearing of 16° from North, the downtown scintillometer is 271°. FMI is Finnish Meteorological Institute at Kumpula. (b) A birds-eye transect along the city-scale scintillometer beam. Height is that above mean sea level using airborne laser database of 1-meter horizontal resolution (National Land of Survey Finland 2010). (c) A cross-section along the city-scale scintillometer beam. (d) Same as b, but for downtown scintillometer beam. (e) Same as c, but for downtown scintillometer beam.

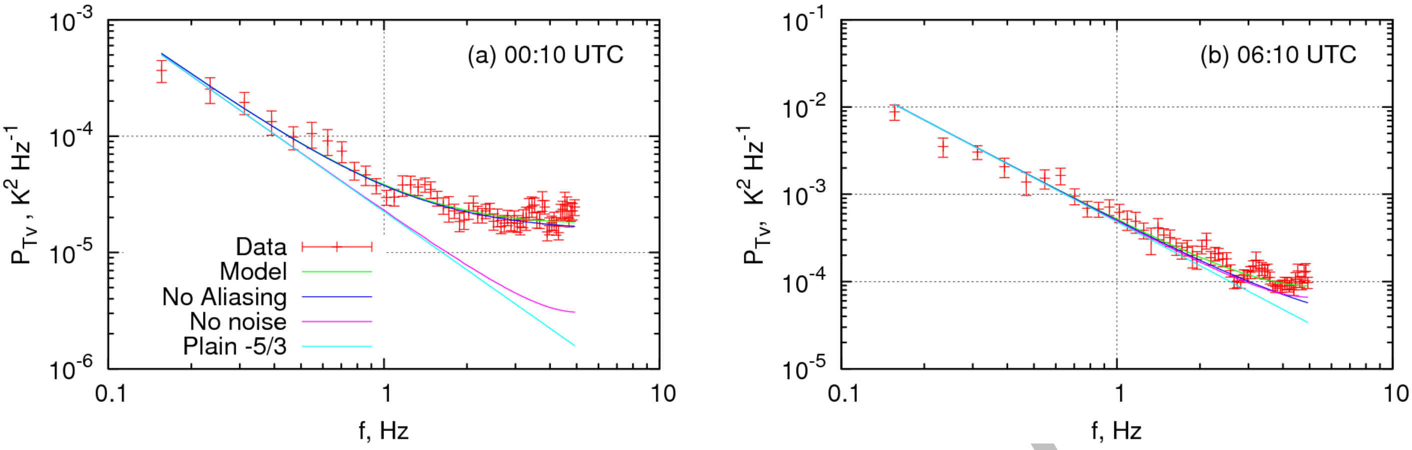

FIG. 2. An example power spectral density from sonic anemometer data for virtual temperature on 14 May 2011 in downtown Helsinki (at Hotel Torni). Shown with fitted spectra: full model, the model without the aliasing term $(f_s - f)^{-5/3}$, the model with β set to 0, and plain –5/3 spectrum.

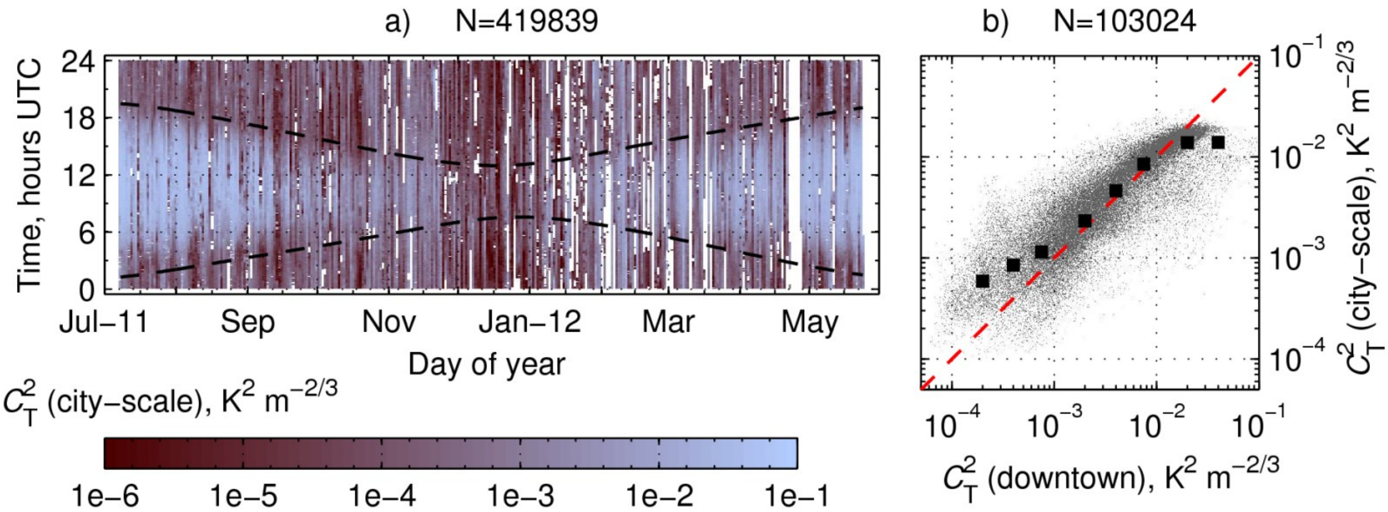

FIG. 3. (a) Seasonal and diurnal cycle for 1-minute-mean temperature structure parameter (shaded scale) from the city-scale scintillometer from July 2011 through May 2012. Sunrise and sunset times are marked (black dashed curves). (b) Comparison of 1-minute mean temperature structure parameter values between the two scintillometers March through May 2012, bin averages are superimposed with black squares.

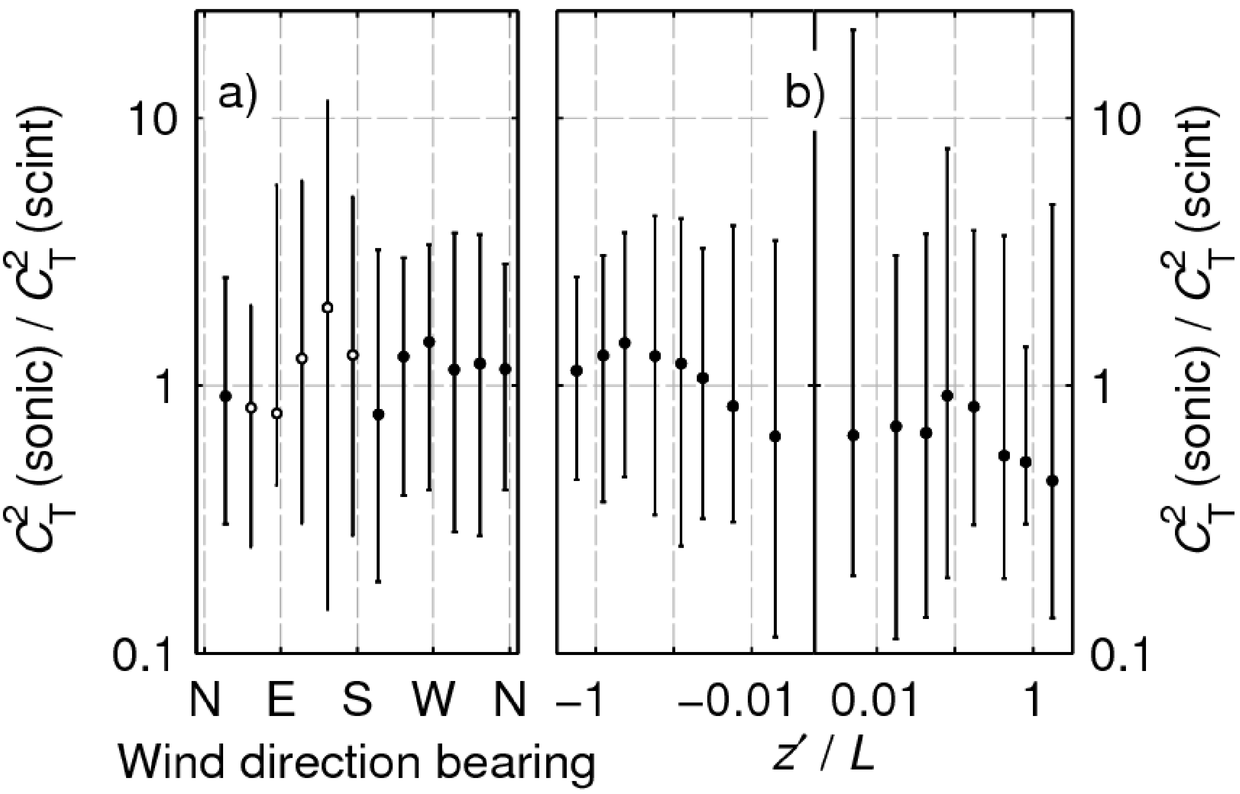

FIG. 4. Ratio of 10-minute-mean data from sonic at Torni to downtown scintillometer during May through June 2012; median values (circles) with 5th and 95th percentiles. (a) For wind-direction bins defined at Torni (flow distortion directions for Torni, 50–185°, are shown as open circles). (b) For stability bins defined at Torni using 30-minute eddy-covariance analysis (flow distortion directions for Torni, 50–185°, are removed).

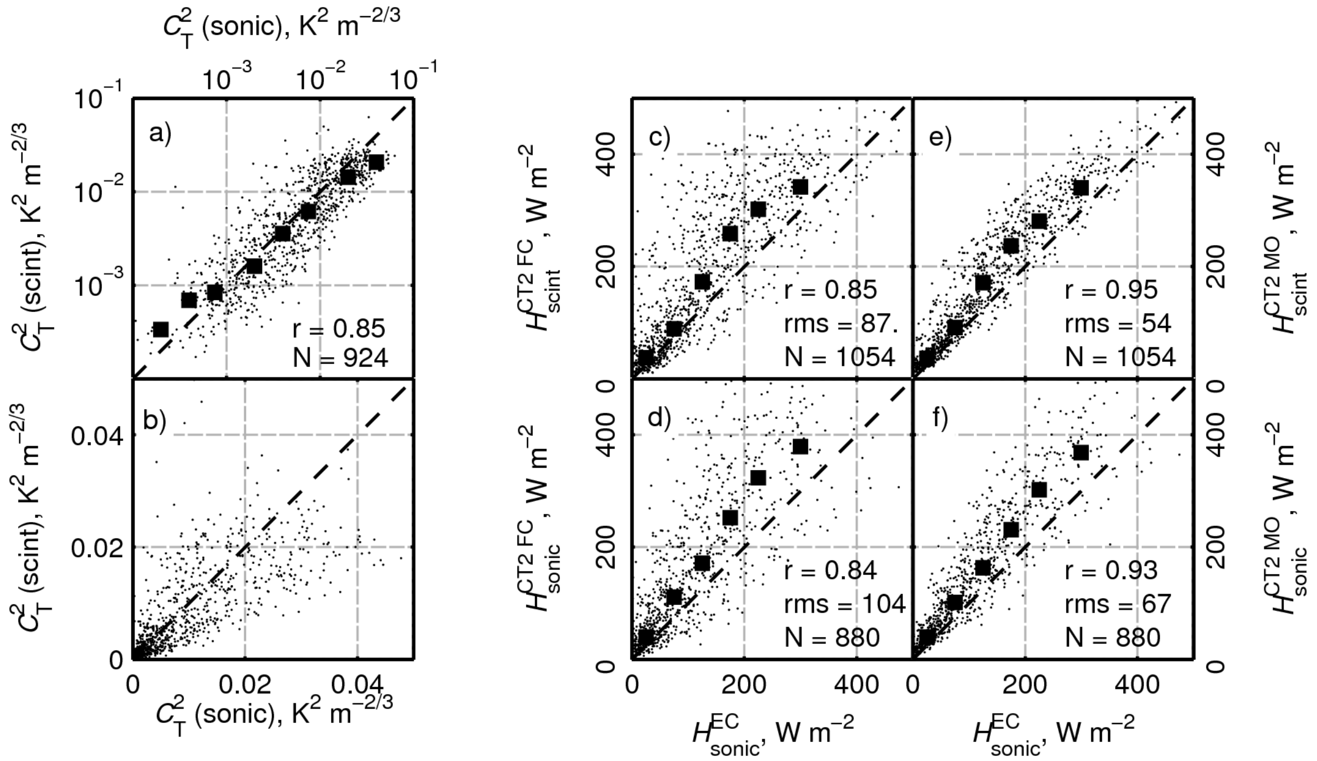

FIG. 5. 30-minute-mean data for downtown May through June 2012, and bin averages are superimposed with black squares (median y-axis value for x-axis bins); the 1:1 line is shown (dashed). The eddy-covariance (EC) data pass the high-quality tests. (a) Comparison of temperature structure parameter values between scintillometer and sonic; (b) same as previous subplot, but on linear scale; (c) EC sensible heat flux compared to sensible heat flux using the free-convection (FC) method with scintillometer temperature structure parameter values; (d) same as previous, but with sonic-derived temperature structure parameter; (e) EC sensible heat flux compared to sensible heat flux with the Monin-Obukhov (MO) theory functional form using scintillometer-derived temperature structure parameter; (f) same as previous subplot, but with sonic-derived temperature structure parameter.

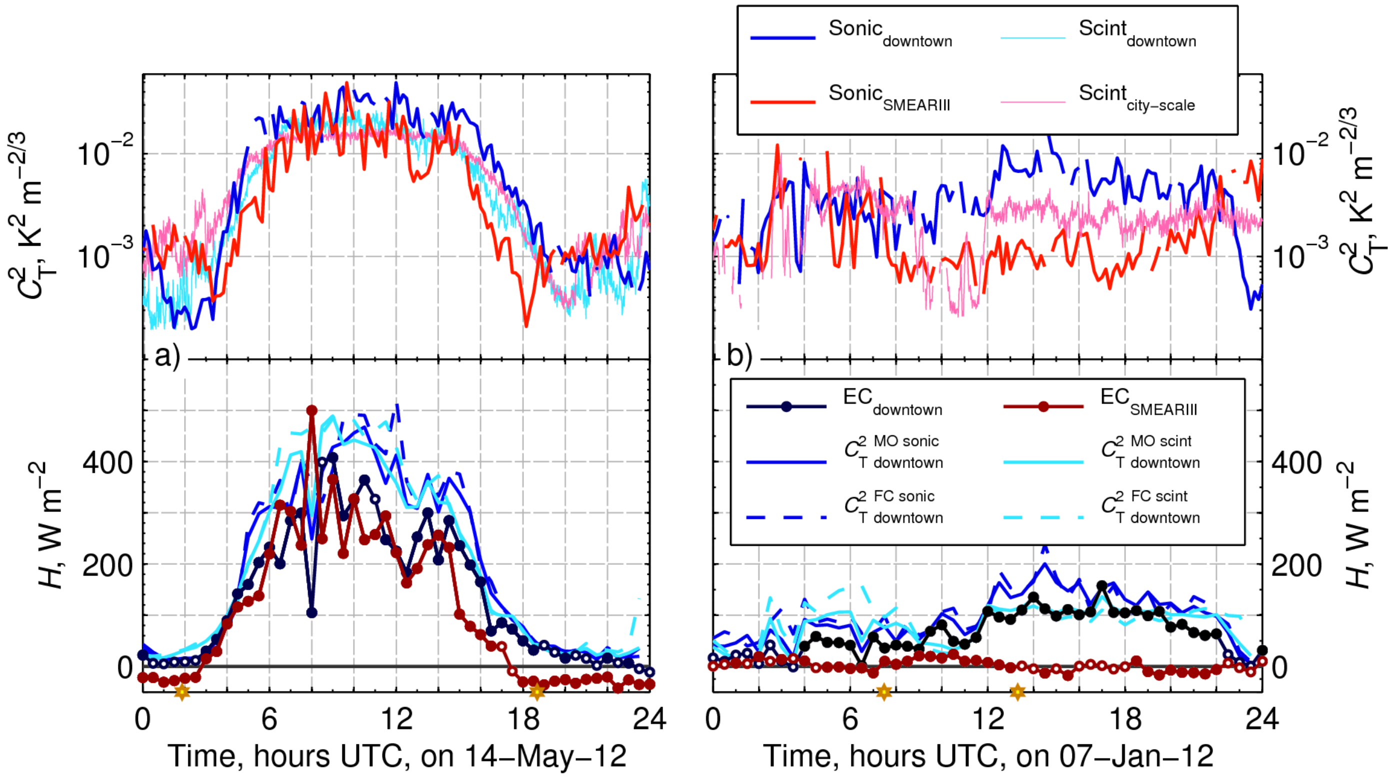

FIG. 6. (a) Temporal evolution on 14 May 2012 of temperature structure parameter (1-minute from scintillometers, 10-minute from sonics) and 30-minute *H*, and (b) 7 January 2012. The legends are the same for horizontal subplots with temperature structure parameter and sensible heat flux. Scint is scintillometer, FC is using the free-convection formulation (Eq. 12), MO is the Monin-Obukhov theory functional form, and EC is using the eddy-covariance method. The EC data pass stringent quality tests (filled circles) or less-stringent quality tests (empty circles). Sunrise and sunset are marked (yellow star).

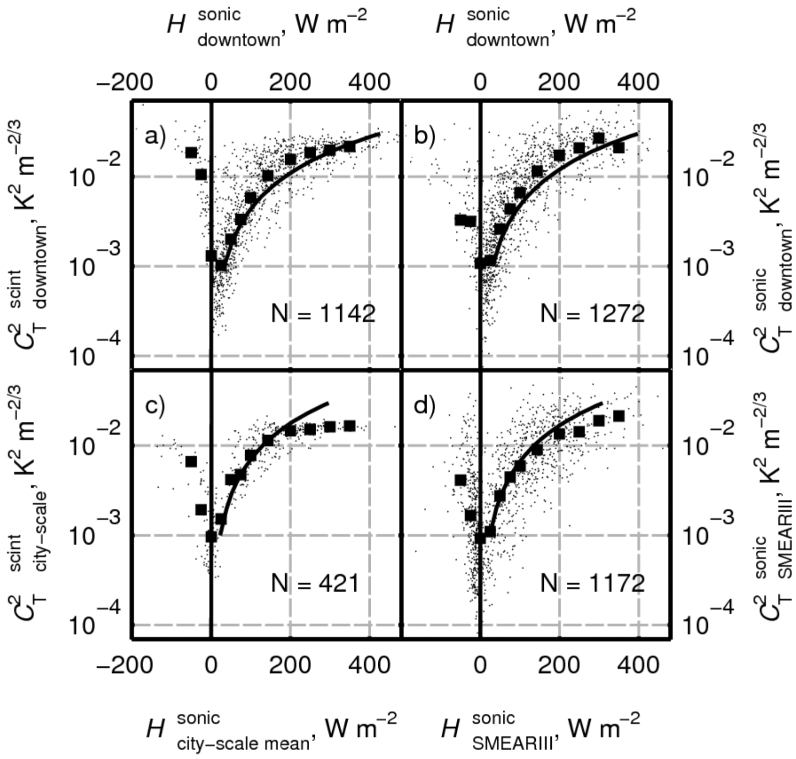

FIG. 7. Sensible heat flux from 30-minute eddy-covariance (stringent quality tests) on x-axes compared to 30-minute temperature structure parameter for different methods for May through June 2012 on y-axes: (a) downtown scintillometer with downtown (Torni) sonic anemometer; (b) Torni sonic anemometer with same sonic; (c) city-scale scintillometer with sonic anemometers (using a mean of Torni and SMEARIII-Kumpula) (NB. less data due to scintillometer downtime from 24th May onwards); (d) SMEARIII-Kumpula sonic anemometer. Bin averages are superimposed with black squares (median y-axis value for x-axis bins). The free-convection relationship (Eq. 12) is shown with the thick curve.

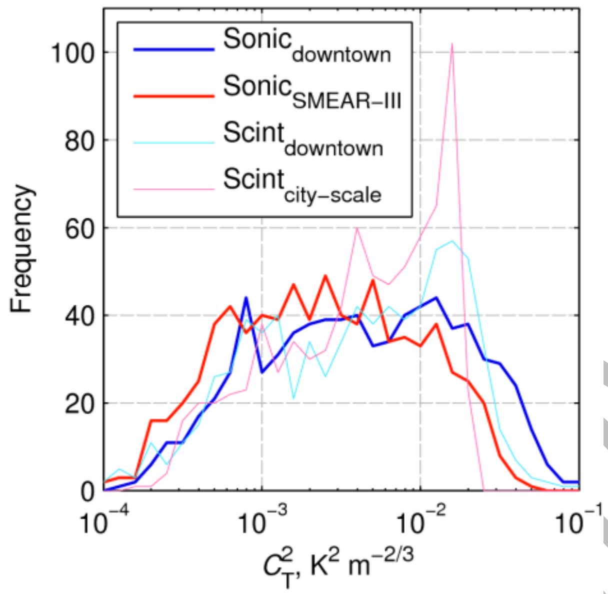

FIG. A1. Histogram for all the 30-minute periods concurrent in all four instruments. These are thus a subset of days from January, February, May, and June 2012. Scintillometer structure parameters were calculated using local temperature and pressure as per equation 3 (i.e. not Scintec SRun software default). Humidity corrections were not applied.